HAL
open science

Oxidation kinetics of Ni metallic films: formation of NiO-based resistive switching structures

L. Courtade, Ch. Turquat, Christophe Muller, J.G. Lisoni, L. Goux, D.J. Wouters, D. Goguenheim, Pascal Roussel, Luc Ortega

To cite this version:

L. Courtade, Ch. Turquat, Christophe Muller, J.G. Lisoni, L. Goux, et al.. Oxidation kinetics of Ni metallic films: formation of NiO-based resistive switching structures. Thin Solid Films, 2008, 516 (12), pp.4083-4092. 10.1016/j.tsf.2007.09.050 . hal-00187467

HAL Id: hal-00187467

https://hal.science/hal-00187467v1

Submitted on 15 Nov 2007

HAL is a multi-disciplinary open access archive for the deposit and dissemination of scientific research documents, whether they are published or not. The documents may come from teaching and research institutions in France or abroad, or from public or private research centers.

L'archive ouverte pluridisciplinaire **HAL**, est destinée au dépôt et à la diffusion de documents scientifiques de niveau recherche, publiés ou non, émanant des établissements d'enseignement et de recherche français ou étrangers, des laboratoires publics ou privés.

Oxidation kinetics of Ni metallic films: formation of NiO-based resistive switching structures

L. Courtade [a], Ch. Turquat [a], Ch. Muller [a,*], J.G. Lisoni [b], L. Goux [b], D.J. Wouters [b], D. Goguenheim [c], P. Roussel [d], L. Ortega [e]

[a] L2MP, Laboratoire Matériaux et Microélectronique de Provence, UMR CNRS 6137, Université du Sud Toulon Var, BP 20132, F-83957 La Garde Cedex, France

[b] IMEC, Interuniversity MicroElectronics Center, Kapeldreef 75, B-3001 Leuven, Belgium

[c] L2MP, Laboratoire Matériaux et Microélectronique de Provence, UMR CNRS 6137, ISEN-Toulon, Maison des Technologies, Place Georges Pompidou, F-83000 Toulon, France

[d] UCCS, Unité de Catalyse et Chimie du Solide, UMR CNRS 8181, ENSCL, BP 90108, F-59652 Villeneuve d'Ascq, France

[e] Laboratoire de Cristallographie, UPR CNRS 5031, BP 166, F-38042 Grenoble Cedex 9, France

Abstract

Resistive switching controlled by external voltage has been reported in many Metal/Resistive oxide/Metal (MRM) structures in which the resistive oxide was simple transition metal oxide thin films such as NiO or TiO_2 deposited by reactive sputtering. In this paper, we have explored the possibility to form NiO-based MRM structures from the partial oxidation of a blanket Ni metallic film using a Rapid Thermal Annealing route, the remaining Ni layer being used as bottom electrode. X-ray diffraction was used to apprehend the Ni oxidation kinetics while transmission electron microscopy enabled investigating local microstructure and film interfaces. These analyses have especially emphasized the predominant role of the as-deposited Ni metallic film microstructure (size and orientation of crystallites) on (i) oxidation kinetics, (ii) NiO film microstructural characteristics (crystallite size, texture and interface roughness) and (iii) subsequent electrical behavior. On this latter point, the as-grown NiO films were initially in the low resistance ON state without the electro-forming step usually required for sputtered films. Above the threshold voltage varying from 2 to 5 V depending on oxidation conditions, the Pt/NiO/Ni MRM structures irreversibly switched into the high resistance OFF state. This irreversibility is thought to originate in the microstructure of the NiO films that would cause the difficulty to re-form conductive paths.

Keywords: oxidation kinetics; resistive switching; bi-stable oxide films; microstructural analysis

PACS number(s): 72.80.Ga, 61.10.Nz, 81.65.Mq, 68.55Ac, 68.55.Jk, 68.37.Lp, 73.40.Rw, 84.37.+q, 85.90.+h

* Electronic mail: christophe.muller@l2mp.fr

1. Introduction

Resistive switching phenomena controlled by external currents or voltages attract a lot of attention for future high-density non-volatile memory devices. The resistive switching-based memory concept enables the integration of the memory element in contacts and interconnects resulting in very small memory cells. Additionally, this concept makes possible a 3-dimensional stacking as recently demonstrated by Baek *et al.* on a multi-layer cross point structured binary oxide resistive random access memory (so-called OxRRAM) for high-density data storage applications [1].

Resistive memory materials range from organic (*e.g.* copper tetracyano quinodimethane) to inorganic materials (*e.g.* chalcogenide alloys, perovskite-type oxides or transition metal oxides) with either metallic or conductive oxide electrodes [2,3]. For inorganic materials, bi-stable switching phenomena have been reported in many simple metal oxides such as Nb_2O_5, Al_2O_3, Ta_2O_5, TiO_2, NiO or ZrO_2 [4-7]. Typical current-voltage I(V) characteristic of Metal/Resistive oxide/Metal (MRM) structures exhibits a drastic change in resistance between a high resistance state (*i.e.* OFF state) and a low resistance state (*i.e.* ON state). Among transition metal oxides, NiO is a promising material due to its compatibility with standard complementary metal-oxide-semiconductor process, its high ON/OFF ratio and simple constituents [4,8]. Resistance switching in crystalline nickel oxide films was observed in 1964 by Gibbons *et al.* [4] and the switching mechanism was explained by a reversible formation/rupture of filamentary conductive paths from the interfaces throughout the NiO film [4,9,10].

In literature, most of the polycrystalline NiO films are deposited by dc (direct current) reactive sputtering on conductive substrates to fabricate MRM structures [10,11]. In this paper, an alternative way was explored using a rapid thermal annealing (RTA) route. Hence, NiO-films were produced from the partial oxidation of a blanket Ni metallic film used as bottom electrode, this approach being similar to the one proposed by Chen *et al.* to form bi-stable CuO_x/Cu stacks [12].

Several process parameters, such as oxidation time, annealing temperature and oxygen partial pressure, were tested to control the growth of NiO films. In addition to the electrical testing, x-ray diffraction experiments enabled apprehending the Ni oxidation kinetics whereas cross-sectional transmission electron microscopy (TEM) was used to observe both the stack microstructure and films interfaces.

2. Experimental details

Ni metallic films with 24 or 100 nm thickness were deposited at room temperature by dc physical vapor deposition (Applied Materials sputtering tool) on $SiO_2/Si_3N_4/Si$ substrates. The film deposition was performed in a base pressure of few mTorr with a dc power source of 400 or 2 000 W for thinner and thicker films respectively (corresponding deposition rates: 10 and 55 nm/min). Different RTA treatments were evaluated to oxidize the Ni films: several process parameters such as oxidation time (from 10 seconds to 30 minutes), annealing temperature (200, 300 and 400°C) and oxygen partial pressure (pure O_2; 20 and 500 ppm O_2) were tested. After the Ni oxidation, a 100 nm thick Pt top electrode (TE) was sputtered through a shadow mask with feature sizes ranging from 1 000 to 160 µm in order to test the electrical behavior of elementary MRM structures.

Local TEM observations coupled with energy dispersive spectroscopy (EDS) analyses were carried out to investigate the microstructure of Ni and NiO films. TEM samples were prepared by focused ion beam (FIB) technique (Ga^+ ions accelerated at 30 kV; a low current ion beam was used to clean the surface at the end of the preparation) and imaging was performed using a Tecnai G^2 (FEI Company) at 200 kV (wavelength of 0.0251 Å). EDS analyses were performed with an EDAX instrument using a Si(Li) detector with a thin beryllium window enabling analysis of elements with $Z > 11$.

X-ray texture analyses were performed on a Siefert 4-circles diffractometer in the Schulz reflection geometry. Copper radiation emitted from an x-ray tube was monochromatized ($\lambda_{K\alpha}$ (Cu)

= 1.5418 Å) and collimated using a bi-dimensional multilayer optical system from Xenocs. Stereographic pole figures were measured by scanning the tilt angle χ between 0 and 90° in steps of 3°, and the azimuthal angle Φ between 0 and 360° in steps of 3°. The pole figures are the projection of the diffraction intensity of a given Bragg reflection as the sample is rotated. The experimental data were corrected for background.

X-ray diffraction technique was used to apprehend the oxidation kinetics of Ni metallic films in different experimental conditions. After each thermal treatment, *ex situ* analyses were performed to check the presence of Ni and NiO phases. Diffraction patterns were registered at room temperature on a Siemens-Bruker D5000 diffractometer configured in Bragg–Brentano geometry, operating with CuK_α radiation and equipped with a diffracted-beam monochromator and Soller slits. Data were collected in the angular range 36 – 46° in 2θ with steps of 0.02° to measure the intensities of (111) Bragg reflections of Ni and NiO phases. Using a profile fitting procedure described elsewhere [13], a peak broadening analysis was performed to extract average size of Ni and NiO crystallites (experimental data were corrected for instrumental broadening).

Besides, *in situ* x-ray diffraction experiments were performed on a Bruker D8 Advance x-ray diffractometer equipped with an Anton-Paar HTK 1200N furnace enabling temperature-dependent measurements under controlled atmosphere. The experimental conditions were as follows: after heating under vacuum from 25°C to the nominal temperature with heating rate of 18°C/min, an isothermal treatment at 400 or 500°C was applied in pure oxygen. Data were collected every 10 seconds using a linear detector (Bruker Vantec 1) over the same angular domain 36 – 46° in 2θ with steps of 0.00741°. A peak broadening analysis was also performed to apprehend the time and temperature-dependent evolution of Ni and NiO crystallite sizes.

Current-Voltage I(V) characteristics were measured on MRM structures with AixACCT TF Analyzer 2000 system using either triangular waveform (typically ± 5 V and 10 Hz; corresponding voltage sweep: 0,2 V/msec) or staircase voltage ramp (voltage step: 0.1 V; dwell time: 1 sec per step). From these measurements, the bi-stable resistive behavior of NiO films was checked and the

switching threshold voltage V_{th} was determined (when a switching occurred). The MRM structures being initially in ON state, the threshold voltage corresponded to the switching from low to high resistance state. Moreover, low (R_{ON}) and high (R_{OFF}) resistances were deduced from the slope of I(V) characteristics. Values of V_{th}, R_{ON} and R_{OFF} were then correlated with process parameters.

3. Microstructure and growth kinetics of NiO films

3.1. Microstructural analysis of Ni and NiO films

Preliminary θ-2θ diffraction patterns were collected on 24 and 100 nm thick Ni layers before the oxidation step. As seen in Fig. 1a, x-ray diffraction profiles of $(111)_{Ni}$ reflection show that the initial 100 nm Ni layer presents a stronger texture along [111] direction as compared to the 24 nm Ni layer. Moreover, interpreting the width of $(111)_{Ni}$ diffraction peak in terms of crystallite size, the 24 nm Ni layer presents much smaller crystallites (≈ 10 nm) as compared to those of the 100 nm Ni layer (≈ 40 nm).

Further x-ray texture analyses were performed on a non-oxidized 100 nm thick Ni layer on $\{111\}_{Ni}$ and $\{200\}_{Ni}$ Bragg reflections. On one hand, the $\{111\}_{Ni}$ pole figure shown in Fig. 1b gives a qualitative description of the orientation of the as-deposited Ni film. The maximum intensity of the $(111)_{Ni}$ Bragg reflection is at the center of the pole figure, the [111] directions being dispersed over a revolution cone centered on the substrate's normal and with about 5° of full width at half maximum. On the other hand, the $\{200\}_{Ni}$ pole figure (Fig. 1c) shows a drastically lower texture with a random orientation of [200] directions around the substrate's normal. Thus, both $\{111\}_{Ni}$ and $\{200\}_{Ni}$ pole figures indicate a strong [111] fibre texture of the Ni layer.

Similar texture analysis was performed on the NiO film obtained from Ni oxidation (100 nm thick layer) at 400°C for 120 seconds in pure O_2. On the $\{111\}_{NiO}$ pole figure (Fig. 1d), the maximum intensity is centered and the rest of the intensity is spread over a wide angular range. This

intensity distribution clearly indicates a texture of the NiO layer along [111] direction even if this texture is much lower than the one observed on Ni metallic film. Consequently, the crystallographic orientation of NiO grains appears to be conditioned by the texture of the underlying Ni film since the NiO films preferentially grow with the [111] direction parallel to the substrate's normal.

TEM experiments were performed on stacks obtained in various oxidation conditions. For instance, Fig. 2a and 2b presents the results of TEM experiments performed on sample coated with a 100 nm thick Ni layer, annealed in pure O_2 at 400°C for 30 seconds and covered with a Pt top electrode. A cross-sectional observation shows a stack of several layers with different contrasts (Fig. 2a). *In situ* x-ray energy dispersive spectrometry (EDS) analysis enabled checking the chemical composition of each film and evidenced a thick Ni-rich layer above Si-rich layer, the upper top layer being Pt. Unfortunately, the EDS detector used was not sensitive to light elements such as oxygen. Consequently, the presence of NiO layer cannot be clearly established from EDS analyses.

To prove the presence of NiO layer, selected area electron diffraction experiments were performed using the smallest available aperture. Although this aperture was still too large to select only one layer, the presence of NiO was confirmed. Indeed, some NiO d-spacings (Powder Diffraction File, PDF no. 47-1049) such as $d_{(111)}$[NiO] differ enough from the d-spacings of the surrounding layers to unambiguously identify the nickel oxide. Using a similar approach with Ni d-spacings (PDF no. 04-0850), the presence of Ni layer was checked. Furthermore, dark field imaging experiments were performed using the diffraction spot corresponding to either $d_{(111)}$[NiO] = 2.412 Å or $d_{(200)}$[Ni] = 1.762 Å (Fig. 2b). These experiments have then definitely confirmed the presence of NiO layer and have enabled locating both Ni and NiO layers within the stack (Fig. 2a).

As shown on TEM cross-section in Fig. 2a, there is a large spread of NiO thicknesses typically ranging from 40 to 75 nm. The Ni layer is dense and constituted by columnar grains with an average size up to 350 nm parallel to the surface. Micro-diffraction experiments (not shown here) suggested that the Ni layer is preferentially oriented with the [111] crystallographic direction

parallel to the substrate's normal, in agreement with the previous x-ray texture analyses. Besides, the Ni/SiO_2 interface is flat and clear of defects whereas Pt/NiO and NiO/Ni interfaces are rough and enclose some voids. The NiO layer is constituted of smaller grains as compared to Ni with a maximum size 120 nm.

3.2. Oxidation kinetics of Ni metallic layer

3.2.1. Ex situ x-ray diffraction to apprehend RTA oxidation

A detailed analysis of NiO/Ni stack formation was performed from x-ray diffraction patterns collected on a 100 nm thick Ni film after RTA oxidation at 400°C in pure O_2 with annealing times ranging from 10 seconds to 30 minutes. In Fig. 3a, concomitant diffracted intensity variations of both Ni (decrease) and NiO (increase) phases are observed with increasing oxidation times. This feature indicates that the Ni metallic film is progressively consumed as the NiO film grows. In addition, the peak profiles were individually adjusted using the program Winplotr [14] to extract the time-dependent evolution of integrated intensity and full width at half maximum (FWHM) of both $(111)_{NiO}$ and $(111)_{Ni}$ reflections. The time-dependent variation of the intensities indicates that the initial extremely rapid oxidation is followed by a slower oxidation rate (not shown here). In addition, the integral breadth β (linked to FWHM) of the $(111)_{NiO}$ Bragg peak decreases with increasing oxidation time (Fig. 3b). The integral breadth β may be interpreted in terms of crystallite size using the Scherrer formulae $\beta = \lambda / (D \times \cos \theta)$, where D is the apparent crystallite size (in the present case, the local strain effect was not taken into account). Consequently, the decrease of β is interpreted as a growth of NiO crystallites along with oxidation times (Fig. 3b).

3.2.2. Oxidation kinetics from in situ time-dependent x-ray diffraction

To complement previous *ex situ* analyses, *in situ* temperature and time-dependent x-ray diffraction experiments were performed on 100 nm thick Ni films annealed at 400 or 500°C in pure

O_2. Before the oxidation step, the Ni metallic films were heated under vacuum in the furnace mounted on the diffractometer and x-ray diffraction patterns were collected from 25°C to 400 or 500°C. As shown in Fig. 4a, the temperature-dependent evolution of the $(111)_{Ni}$ Bragg reflection exhibits a drastic intensity increase. Using an individual profile fitting procedure, the integrated intensity (Fig. 4b) and integral breadth β (Fig. 4c, left) were extracted. Both evolutions indicate a further crystallization of Ni layer during heating and the decrease of β above 100°C may be interpreted as an increase of the average Ni crystallite size (Fig. 4c, right). The same tendency was observed for sample heated up to 500°C.

In a second step, time-dependent x-ray diffraction patterns were collected in pure O_2 at constant temperature for 15 hours. The scanned angular range was limited to 36–46° in 2θ, domain that contains the $(111)_{Ni}$ and $(111)_{NiO}$ reflections. Whatever the isotherm, concomitant variation between both Ni and NiO intensities was observed with increasing oxidation times as illustrated in Fig. 5a for isotherm at 400°C. Figure 5b presents the time-dependent variation at 400°C of integrated intensity for $(111)_{NiO}$ and $(111)_{Ni}$ Bragg peaks. These evolutions indicate that the Ni metallic film is progressively consumed as the NiO film grows up to the total consumption of the Ni layer. The same kind of evolution was observed at 500°C with faster oxidation kinetics. Figure 6a shows the time-dependent variation, at 400 and 500°C, of the $(111)_{NiO}$ integrated intensity ratio $I(t) / I_\infty(t \rightarrow \infty)$ between time t and final time (*i.e.* $t \rightarrow \infty$) after total Ni consumption. These ratios qualitatively point out that the Ni oxidation rate increases with increasing annealing temperature.

Figure 6b shows, at 400 and 500°C, the time-dependent increase of NiO average crystallite size D deduced from the decrease of the $(111)_{NiO}$ integral breadth β. Isothermal nucleation/growth process of particles is usually described by the Johnson-Mehl-Avrami-Kolmogorov (JMAK) theory [15-17]. This model gives the time-dependent evolution of the volume V(t) of a nucleating and growing phase. In the present case, the evolution in time of NiO crystallite size D has been fitted using a JMAK-type equation: $D(t) = D_\infty [1 - \exp(- k \times t^n)]$, where D_∞ corresponds to the final

crystallite size when $t \rightarrow \infty$. The satisfactory fitting of experimental data shown in Fig. 6b clearly indicates that the growth of NiO crystallites follows the JMAK model. Table 1 summarizes the parameters of the JMAK model for each temperature. The parameters n and k are respectively the JMAK coefficient and the growth rate constant depending on temperature. The growth rate constant k is around 0.96 at 400°C while at 500°C, k equals 1.42. Besides, the crystallite size is also influenced by the temperature: at 400°C, $D_\infty \approx 26$ nm while $D_\infty \approx 32$ nm at 500°C. These results clearly show that growth of NiO crystallites is significantly accelerated at 500°C.

3.2.3. Comparison of RTA and in situ oxidation conditions

Inset in Fig. 6b illustrates the growth of NiO crystallites *versus* oxidation times (< 2 hours) (i) for pre-treated Ni films at 400 or 500°C (*in situ* diffraction experiments) and (ii) for a Ni layer directly subjected to the oxidizing atmosphere (*ex situ* diffraction experiments). At 400°C, the rather different growth rate constants k indicate that the oxidation kinetics is much faster for RTA route (Table 1). The main difference between these two sets of conditions stands in the pre-treatment of Ni metallic layer prior to oxidation. Furthermore, at 400°C after 30 minutes in pure O_2, the crystallite size is about 14 nm when the Ni film is pre-treated under vacuum whereas it is of 21 nm without pre-treatment. Hence, these analyses show that the oxidation kinetics of Ni layer strongly depends on its own microstructure, which is modified by the thermal pre-treatment.

4. Electrical behavior of NiO films obtained in various conditions

4.1. Typical switching characteristic

Figure 7 shows a typical current-voltage I(V) switching characteristic measured with a staircase voltage ramp on a Pt/NiO/Ni stack. The measurements were performed on an initial 100 nm thick Ni layer oxidized in pure O_2 using RTA at 400°C for 10 seconds. For a voltage sweep $0 \rightarrow 4\ V \rightarrow 0$

→ – 4 V → 0, no switching occurs and the high current response is indicative of the initial low resistance state. As the voltage is ramped up to 4.5 V, the current abruptly decreases at 4.2 V pointing out a resistance switching of the MRM structure from a low (R_{ON} = 55 Ω) to a high resistance state (R_{OFF} = 2 360 Ω). In this latter case, the switching was irreversible, the structure remaining in OFF state whatever the bias imposed.

The Pt top electrode area dependence of resistance switching was also studied: in reducing TE diameter from 540 to 160 µm, the current in the low resistance (LRS) state remains quite unchanged whereas a decrease of one order of magnitude is observed in the high resistance state (HRS). These results indicate that the conduction in HRS is strongly dominated by the area of top electrode whereas the formation of filamentary paths in the oxide can be proposed to explain the conduction in LRS. Besides, it has been mentioned in the previous paragraph that the MRM structures systematically turn off around 4.2 V in applying a positive voltage to the bottom electrode with a sweep of 0.2 V/msec. In decreasing the voltage sweep, the current through the structure increases whereas the threshold voltage decreases (*e.g.* for a sweep of 0.02 V/msec, the switching is observed at 3.7 V). Consequently, the opposite variations of current level and threshold voltage seem to be in favor of a heating Joule effect with a subsequent destruction of filaments in LRS and a switching to HRS.

4.2. Influence of annealing time and temperature under pure oxygen

I(V) measurements were performed on samples coated with a 24 or 100 nm thick Ni layer, oxidized in pure O_2 at different temperatures (200, 300 and 400°C) with RTA times ranging from 10 seconds to 5 minutes. The observed electrical behavior was systematically correlated with *ex situ* x-ray diffraction patterns enabling detection of Ni and/or NiO phases. Fig. 8a shows that the threshold voltage V_{th} increases along with annealing time whatever the initial thickness of Ni film.

For samples with a 100 nm thick Ni layer, an annealing at 300°C or above in pure O_2 is required to at least partially oxidize the metallic film and to form NiO-based structures exhibiting a resistance switching with threshold voltages ranging from 3.5 to 5 V (Table 2a). Indeed, the observation of $(111)_{NiO}$ Bragg reflection for RTA at 300 and 400°C is in agreement with the formation of a bi-stable NiO layer whereas the absence of NiO phase for RTA at 200°C explains the lack of switching behavior. Moreover, the threshold voltage V_{th} increases along with the annealing temperature: for instance after 180 seconds of oxidation, V_{th} raises from 4.3 V at 300°C to 5 V at 400°C.

For samples with initial 24 nm thick Ni layer, V_{th} follows the same tendency since it increases along with annealing time and temperature (Fig. 8a). For instance, after 180 seconds of annealing, V_{th} increases from 3.1 V at 200°C to 3.8 V at 300°C. Furthermore, it is observed that no switching occurs when the Ni films were annealing at 400°C for times larger than 30 seconds. X-ray diffraction experiments have shown that, in these conditions, the Ni metallic film is fully consumed (with subsequent disappearance of bottom electrode). In this latter case, electrical measurements are impossible. Besides the threshold voltage, the evolution of R_{ON} and R_{OFF} resistances deduced from the slope of I(V) curves measured on samples annealed at 300°C shows a very slight increase with annealing time although the R_{OFF}/R_{ON} ratio remains quite unchanged (Fig. 8b). The average R_{OFF}/R_{ON} ratio is around 55 for samples with an initial 100 nm thick Ni layer annealed at 300°C, whereas it is only around 15 for samples with 24 nm thick Ni layer. Therefore, in the perspective of memory devices, 100 nm thick Ni layers provide a large memory window enabling a better discrimination between ON and OFF states. In contrast, the lower threshold voltages measured on 24 nm thick Ni layers oxidized at moderate temperature with short annealing times would match the low-voltage application requirements.

4.3. Influence of oxidizing atmosphere

Different oxidizing atmospheres (20 and 500 ppm of O_2; pure O_2) were tested on samples coated with initial 24 or 100 nm thick Ni layer and annealed using RTA at 200 and 400°C for 30 seconds and 3 minutes. Once again I(V) characteristics were systematically correlated with x-ray diffraction patterns. Figure 9 presents the distribution of threshold voltages V_{th} measured in different experimental conditions. The main trend is the augmentation of V_{th} with increasing oxygen partial pressure: V_{th} varies from 2.2 V (24 nm thick Ni layer annealed at 200°C for 30 seconds under 20 ppm of O_2) to 5 V (100 nm thick Ni layer annealed at 400°C for 180 seconds in pure O_2). It is worth to note that in few cases no switching was observed for 24 nm thick Ni layers (Table 2b). For instance at 400°C, whatever the oxygen partial pressure, the annealing time has to be limited to 30 seconds to prevent the total oxidation of Ni layer (checked by x-ray diffraction). In contrast, for lower temperatures (*i.e.* 200 and 300°C), the Ni layer is only partially oxidized whatever the annealing time and oxygen partial pressure and a switching is observed.

As partial conclusion, Fig. 9 helps to establish the experimental conditions required to form bi-stable NiO films with switching voltages which may be easily tailored in monitoring annealing time and/or O_2 partial pressure.

5. Discussion

In this section, both microstructural and electrical characteristics of Pt/NiO/Ni MRM structures are discussed in correlation with the experimental conditions. Tables 2a and 2b gather the experimental conditions, the presence of Ni and/or NiO layers (detected by x-ray diffraction) and the threshold voltage of the MRM structures when switching was observed.

5.1. Impact of Ni microstructure on oxidation kinetics

Electrical testing presented in previous section revealed major differences in the switching behavior which may be linked to the Ni microstructure before oxidation step. Indeed, a resistive switching occurs on a 24 nm Ni layer oxidized at 200°C whereas it is not observed on a 100 nm Ni film annealed in the same conditions (*cf.* Tables 2a and 2b). This peculiar behavior may find its origin in the thickness-dependent microstructure of Ni layer which influences the oxidation kinetics. As shown in Fig. 1a, the 24 nm thick Ni layer presents much smaller crystallites and a lower texture along $[111]_{Ni}$ direction as compared to the 100 nm thick Ni layer. Consequently, the growth kinetics of NiO film seems to depend on the texture and crystallite size of the initial Ni metallic layer. Several arguments may support this hypothesis:

- Firstly, x-ray texture analyses (Fig. 1d) showed a fibre texture of NiO film along the [111] direction (*cf.* section 3.1.). This result is in good agreement with the work of Czerwinski *et al.* which showed that the stronger the $[111]_{Ni}$ substrate texture, the stronger the $[111]_{NiO}$ oxidized layer texture became after oxidation [18]. In contrast, López-Beltrán *et al.* obtained texture-free polycrystalline NiO layer from the oxidation of a weakly textured Ni film [19].
- Second, concerning the Ni film texture, Czerwinski *et al.* and Peraldi *et al.* have demonstrated the important role of crystallographic orientation of nickel on its oxidation kinetics [18,20-22]. Hence, a strong [111] texture of Ni leads to formation of highly protective and slow growing NiO film, *i.e.* a weaker Ni texture significantly decreases the resistance to the oxidation.
- Finally, Graham *et al.* demonstrated that the oxidation rate is strongly dependent on the Ni surface morphology [23,24]. Moreover, at lower temperatures, the influence of oxygen transport increases through short circuit paths, such as grain boundaries and dislocations [23,25,26]. As a result, smaller Ni crystallites result in a larger amount of grain boundaries which may facilitate the oxygen diffusion and accelerate the NiO formation.

Consequently, the non-oxidation of 100 nm thick Ni film at 200°C (with subsequent lack of switching) may find its origin (i) in a stronger $[111]_{Ni}$ texture that increases the resistance to

oxidation and (ii) in larger crystallites that decrease the amount of grain boundaries and limit oxygen diffusion.

Besides, as seen in inset of Fig. 6b, the comparison of time-dependent growth of NiO crystallites (extracted from *ex situ* and *in situ* x-ray diffraction experiments) confirms again the influence of Ni microstructure on the NiO growth. When the Ni metallic film is annealed under vacuum prior to oxidation, a further crystallization occurs with an enhancement of $[111]_{Ni}$ texture and a growth of Ni crystallites (*cf.* Figs. 4b and 4c). In contrast, the RTA conditions lead to a rather different situation with two competitive mechanisms that simultaneously occur: Ni crystallization with subsequent changes in the microstructure; growth of NiO film with progressive consumption of the Ni layer. Thus, the different "history" of Ni layer before oxidation may explain the faster kinetics (*cf.* Table 1) observed in RTA conditions in which metallic layer is directly subjected to the oxidizing atmosphere without pre-treatment.

To conclude, in agreement with previous published works [23-26], the Ni surface morphology and its thermal treatment prior to the oxidation radically change the growth kinetics of the NiO film. Consequently, the present experiments emphasize the importance of thermal pre-treatment in order to avoid the competition between Ni crystallization and oxidation.

5.2. Initial ON state

As compared to sputtered films reported in literature, the NiO films obtained from Ni oxidation are initially in ON state without special electro-forming generally required to reach the conductive state. Oxygen content in oxide films may explain such a behavior. Varying oxygen content in sputtering gas mixture, several authors have shown a drastic modification of the electrical properties of Ni_xO films from a metallic behavior (highly Ni-excess films) at low oxygen content (< 5 % of oxygen in sputtering gas) to a monostable threshold switching (Ni-deficient films) at high oxygen content (> 20 %), the memory switching region being limited to intermediate oxygen

contents (10-17%) [27,28]. The comparison of the cubic cell parameter of films obtained in pure oxygen (a = 4.18 Å) with those of Ni-deficient (a = 4.23 Å) and Ni-excess (a = 4.17 Å) films suggests that nickel oxide films obtained from Ni oxidation are close to the Ni-excess region within memory switching area [27,28]. Moreover, the vicinity of the metallic behavior region may certainly explain the initial conductive state.

5.3. Irreversible switching

On the basis of the previous discussion, one could expect a reversible switching of NiO-based structures. On the contrary the MRM structures remained in the OFF state after the first and unique switching. This irreversibility certainly originates in the roughness of NiO/Ni and Pt/NiO interfaces seen on TEM cross-section images (Fig. 2a). Indeed, the TEM observations have revealed that the Ni metal surface is covered by a continuous but irregular oxide layer with thicknesses ranging from 40 to 75 nm. This latter characteristic may have a crucial role on the reversibility of switching since several authors have attributed the switching to the formation/rupture of conductive paths near the interface [4,9]. During oxidation, the growth of the NiO oxide film is rather non-uniform as a consequence of different growth rates for different Ni grain orientations. Indeed, Peraldi *et al.* have demonstrated the important role of the crystallographic orientation of nickel on the oxidation kinetics [21,22]. For instance, oxidation of the (100) nickel face is more rapid than oxidation of (110), (111), and (112) faces. Once again, it appears crucial to stabilize the Ni film microstructure before oxidation step in order to decrease the roughness of the NiO film.

Finally, in previous works, Haugsrud mentioned the existence of microfissures within the NiO oxide obtained from Ni oxidation at high temperatures [26,29]. Several main routes were suggested to account for the presence of microfissures [29]. Based on these results, one can propose the existence of such microfissures within the NiO film which may explain the difficulty to re-form the conductive paths after switching. These microfissures may also lead to a partial delamination at the

interface between Ni and NiO films, such a delamination being sometimes observed during TEM cross-section sample preparation by mechanical polishing (Tripod technique).

6. Conclusion

In this paper, the oxidation kinetics of Ni metallic films were apprehended in order to form NiO layers exhibiting a voltage-induced resistive switching within Pt/NiO/Ni MRM structures. Process parameters (temperature, annealing time and oxidizing atmosphere) of Rapid Thermal Annealing route were tested to achieve oxidation. Different thermal treatments were selected to oxidize the metallic film with conditions (i) preventing the complete consumption of Ni film used as bottom electrode and (ii) producing bi-stable oxide films. With these experimental conditions, the as-grown NiO films were initially in the low resistance ON state without special electro-forming usually required for sputtered NiO films. The obtaining of Ni-excess oxide films may explain the initial metallic behavior. Nevertheless, above a threshold voltage, varying from 2 to 5 V depending on the oxidizing conditions, the MRM structures irreversibly switched into a high resistance OFF state. This irreversibility may be linked to the roughness of NiO/Ni and Pt/NiO interfaces due to a non-stabilized Ni film microstructure prior to oxidation.

In the perspective of memory devices, further microstructural and electrical analyses are required to decrease the threshold voltage of reversible memory elements. Currently, new experimental conditions are evaluated in order to control the Ni crystallization prior to oxidation and alternative routes for Ni oxidation such as plasma treatment under N_2O or O_2 is explored. Finally, fully integrated bi-stable NiO/Ni stacks in via structures will be fabricated and the stability of the MRM structures in conditions close to those used in the back-end process will be checked.

Acknowledgments

This work is partially supported by EC through the Marie Curie project APROTHIN ("Advanced PROcess Technologies for Horizontal INtegration", FP6-514221).

References

[1] I.G. Baek, D.C. Kim, M.J. Lee, H.-J. Kim, E.K. Yim, M.S. Lee, J.E. Lee, S.E. Ahn, S. Seo, J.H. Lee, J.C. Park, Y.K. Cha, S.O. Park, H.S. Kim, I.K. Yoo, U. Chung, J.T. Moon, B.I. Ryu, Int. Electron Devices Meeting Tech. Dig. (2005) 750.

[2] R. Müller, S. De Jonge, K. Myny, D.J. Wouters, J. Genoe, P. Heremans, Solid-State Electron. 50 (2006) 601.

[3] S.L. Cho, J.H. Yi, Y.H. Ha, B.J. Kuh, C.M. Lee, J.H. Park, S.D. Nam, H. Horii, B.K. Cho, K.C. Ryoo, S.O. Park, H.S. Kim, U-In Chung, J.T. Moon, B.I. Ryu, VLSI Technology Tech. Dig., (2005) 96.

[4] J.F. Gibbons, W.E. Beadle, Solid-State Electron. 7 (1964) 785.

[5] B.J. Choi, D.S. Jeong, S.K. Kim, C. Rohde, S. Choi, J.H. Oh, H.J. Kim, C.S. Hwang, K. Szot, R. Waser, B. Reichenberg, S. Tiedke, J. Appl. Phys. 98 (2005) 033715.

[6] C. Rohde, B.J. Choi, D.S. Jeong, S. Choi, J-S. Zhao, C.S. Hwang, Appl. Phys. Lett. 86 (2005) 262907.

[7] L. Courtade, Ch. Turquat, Ch. Muller, J.G. Lisoni, L. Goux, D.J. Wouters, D. Goguenheim, IEEE Proceedings of the Non Volatile Memory Technology Symposium (2006) 94.

[8] S. Seo, M.J. Lee, D.H. Seo, E.J. Jeoung, D.-S. Suh, Y.S. Joung, I.K. Yoo, I.R. Hwang, S.H. Kim, I.S. Byun, J.-S. Kim, J.S. Choi, B.H. Park, Appl. Phys. Lett. 85 (2004) 5655.

[9] I.H. Inoue, M.J. Rozenberg, S. Yasuda, M.J. Sanchez, M. Yamazaki, T. Manago, H. Akinaga, H. Takagi, H. Akoh, Y. Tokura, IEEE Proceedings of the Non Volatile Memory Technology Symposium (2005) 131.

[10] D.C. Kim, S. Seo, S.E. Ahn, D.-S. Suh, M.J. Lee, B.-H. Park, I.K. Yoo, I.G. Baek, H.-J. Kim, E.K. Yim, J.E. Lee, S.O. Park, H.S. Kim, U-In Chung, J.T. Moon, B.I. Ryu, Appl. Phys. Lett. 88 (2006) 202102.

[11] G. Baek, M.S. Lee, S. Seo, M.J. Lee, D.H. Seo, D.-S. Suh, J.C. Park, S.O. Park, H.S. Kim, I.K. Yoo, U-In Chung, J.T. Moon, Int. Electron Devices Meeting Tech. Dig. (2004) 587.

[12] A. Chen, S. Haddad, Y.-C. Wu, T.-N. Fang, Z. Lan, S. Avanzino, S. Pangrle, M. Buynoski, M. Rathor, W. Cai, N. Tripsas, C. Bill, M. Van Buskirk, M. Taguchi, Int. Electron Devices Meeting Tech. Dig. (2005) 746.

[13] Ch. Muller, F. Jacob, Y. Gagou, E. Elkaim, J. Appl. Cryst. 36 (2003) 880.

[14] T. Roisnel, R. Rodriguez-Carvajal, Mater. Sci. Forum 378-381 (2001) 118.

[15] S.F. Hulbert, J. Br. Ceram. Soc. 6 (1969) 11.

[16] E.J. Mittemeijer, J. Mater. Sci. 27 (1992) 3977.

[17] M. Isa, J.C. Valmalette, Ch. Muller, C. Leroux, Chem. Mater. 7 (2005) 5920.

[18] F. Czerwinski, J. A. Szpunar, Corros. Sci. 41 (1999) 729.

[19] A.M. López-Beltrán, A. Mendoza-Galván, Thin Solid Films 503 (2006) 44.

[20] F. Czerwinski, J.A. Szpunar, Acta Mater. 46 (1998) 1403.

[21] R. Peraldi, D. Monceau, B. Pierragi, Oxid. Met. 58 (2002) 275.

[22] R. Peraldi, D. Monceau, S. Jean, B. Pierragi, Mater. High Temp. 20 (2003) 649.

[23] M.J. Graham, M. Cohen, J. Electrochem. Soc. 119 (1972) 879.

[24] M.J. Graham, R.J. Hussey, M. Cohen, J. Electrochem. Soc. 119 (1973) 1523.

[25] L. Berry, J. Paidassi, Mem. Sci. Rev. Met. 65 (1968) 651.

[26] R. Haugsrud, Corros. Sci. 45 (2003) 211.

[27] J.-W. Park, J.-W. Park, K. Jung, M.K. Yang, J.-K. Lee, J. Vac. Sci. Technol. B 24 (2006) 2205.

[28] M.J. Lee, S. Seo, D. Seo, E. Jeong, I. K. Yoo, Integr. Ferroelectr. 68 (2005) 19.

[29] R. Haugsrud, Corros. Sci. 45 (2003) 1289.

Table captions

Table 1. Parameters of the Johnson-Mehl-Avrami-Kolmogorov (so-called JMAK) equation: $D(t) = D_\infty [1 - \exp(- k \times t^n)]$ which may describe the nucleation/growth process of NiO crystallites in various experimental conditions (RTA conditions or *in situ* oxidation).

Table 2. Sum up of electrical behavior correlated with the presence of NiO and/or Ni phases checked by x-ray diffraction. The initial Ni thickness is 100 nm (a) or 24 nm (b) (NSW = no switching; SW = switching; corresponding V_{th} is given when a resistive switching is observed).

	T (°C)	D_∞ (nm)	k	n
RTA conditions	400	19.6	8.8	0.35
In situ oxidation	400	26.5	1.0	0.41
	500	32.4	1.4	0.22

Table 1

(a)		200°C			300°C			400°C		
		30 s	180 s	300 s	30 s	180 s	300 s	30 s	180 s	300 s
PO_2	Pure O_2	NSW – Ni	NSW – Ni	NSW – Ni	SW 3.8 V NiO/Ni	SW 4.3 V NiO/Ni	SW 4.7 V NiO/Ni	SW 4.4 V NiO/Ni	SW 4.9 V NiO/Ni	SW 5 V NiO/Ni
	500 ppm O_2	NSW – Ni	NSW – Ni					SW 3.3 V NiO/Ni	SW 3.8 V NiO/Ni	
	20 ppm O_2	NSW – Ni	NSW – Ni					SW 2.9 V NiO/Ni	SW 3.3 V NiO/Ni	

(b)		200°C			300°C			400°C		
		30 s	180 s	300 s	30 s	180 s	300 s	30 s	180 s	300 s
PO_2	Pure O_2	SW 3.1 V NiO/Ni	SW 3.2 V NiO/Ni	SW 3.3 V NiO/Ni	SW 3.3 V NiO/Ni	SW 3.7 V NiO/Ni	SW 3.8 V NiO/Ni	NSW – NiO	NSW – NiO	NSW – NiO
	500 ppm O_2	SW 2.8 V NiO/Ni	SW 3.1 V NiO/Ni					SW 3.2 V NiO/Ni	NSW – NiO	
	20 ppm O_2	SW 2.2 V NiO/Ni	SW 2.7 V NiO/Ni					SW 2.5 V NiO/Ni	NSW – NiO	

Table 2

Figure captions

Fig. 1. (a) Comparison of $(111)_{Ni}$ Bragg reflections for 24 and 100 nm thick Ni layers prior to oxidation (θ-2θ diffraction patterns). (b) $\{111\}_{Ni}$ and (c) $\{200\}_{Ni}$ pole figures of a non-oxidized 100 nm thick Ni layer. (d) $\{111\}_{NiO}$ pole figure of NiO film formed from oxidation of Ni layer (100 nm thick) at 400°C for 120 seconds in pure O_2.

Fig. 2. (a) TEM cross-section of the stack Pt/NiO/Ni/SiO_2/Si_3N_4/Si: the NiO film was obtained from oxidation of Ni layer using RTA at 400°C for 30 seconds in pure O_2. The upper layer protects the stack during before FIB cutting. (b) Selected area electron diffraction pattern and dark field images corresponding to $(111)_{NiO}$ and $(200)_{Ni}$ Bragg spots.

Fig. 3. (a) Evolution *versus* oxidation time of $(111)_{NiO}$ (on left) and $(111)_{Ni}$ (on right) Bragg reflections. (b) Annealing time-dependent evolution of integral breadth β of $(111)_{NiO}$ Bragg reflection and corresponding average size of NiO crystallites.

Fig. 4. (a) Temperature-dependence of diffraction patterns recorded under vacuum from 25 to 400°C (100 nm thick Ni layer). (b) Corresponding temperature-dependent evolution of $(111)_{Ni}$ integrated intensity. (c) Using a profile fitting procedure, diffraction peak broadening analysis was performed to extract the integral breadth β of the $(111)_{Ni}$ reflection which may be interpreted in terms of Ni crystallite size.

Fig. 5. (a) Time-dependent evolution of diffraction patterns recorded at isotherm 400°C in pure O_2 and showing concomitant evolutions of $(111)_{Ni}$ and $(111)_{NiO}$ Bragg reflections. (b) Corresponding evolution of integrated intensities.

Fig. 6. (a) Evolution *versus* oxidation time of integrated intensity ratio I(t) / I(t→∞) of $(111)_{NiO}$ Bragg reflection measured at 400 and 500°C. (b) Time-dependent growth of NiO apparent crystallite size deduced from the integral breadth β of $(111)_{NiO}$ reflection measured at 400 and 500°C. The solid lines are the curves calculated from the JMAK model (see text for details). Inset compares the evolution of NiO crystallite size (t < 2 hours) for pre-treated Ni films at 400 and 500°C and for a Ni layer directly subjected to the oxidizing atmosphere at 400°C.

Fig. 7. Typical I(V) switching characteristics of the Pt/NiO/Ni MRM structures: the NiO film was obtained from oxidation of a 100 nm thick Ni layer using RTA at 400°C for 10 seconds in pure O_2.

Fig. 8. (a) Evolution of threshold voltage (V_{th}) as a function of the annealing time for Pt/NiO/Ni MRM structures. I(V) characteristics were measured on samples with initial 24 or 100 nm thick Ni layers, annealed under pure O_2 at different temperatures (200, 300 and 400°C) from 10 to 300 seconds. No switching was observed for 100 nm thick Ni layer annealed at 200°C. (b) Typical annealing time-dependent variation of low (R_{ON}) and high (R_{OFF}) resistances of 24 or 100 nm thick Ni layer oxidized at 300°C in pure O_2.

Fig. 9. Distribution of threshold voltages (V_{th}) for Pt/NiO/Ni MRM structures produced under different oxidizing atmospheres (RTA at 200 and 400°C for 30 and 180 seconds).

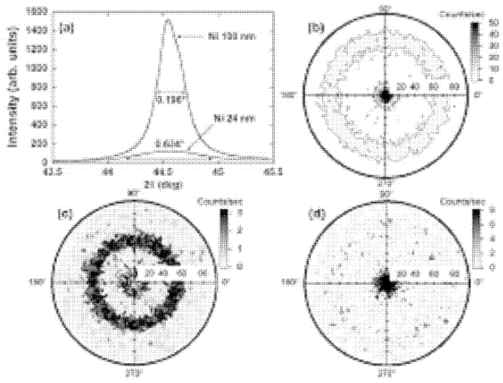
Intensity (arb. units)
[a]
Ni 100 nm
Ni 24 nm
2θ (deg)
[b]
[c]
[d]
Counts/sec

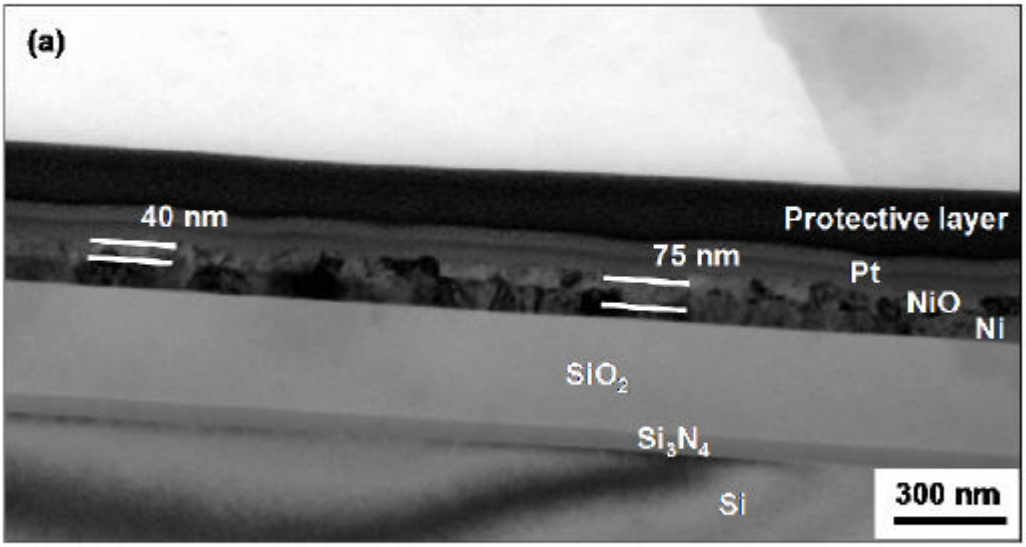
(a)
40 nm
Protective layer
75 nm
Pt
NiO
Ni
SiO2
Si3N4
Si
300 nm

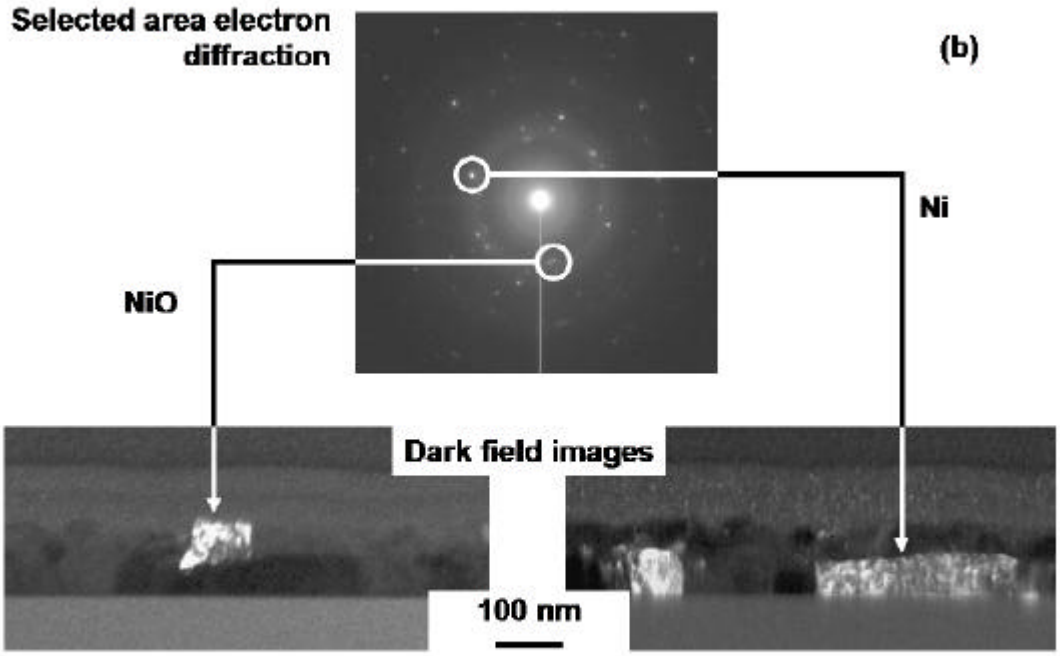
Selected area electron diffraction
(b)
Ni
NiO
Dark field images
100 nm

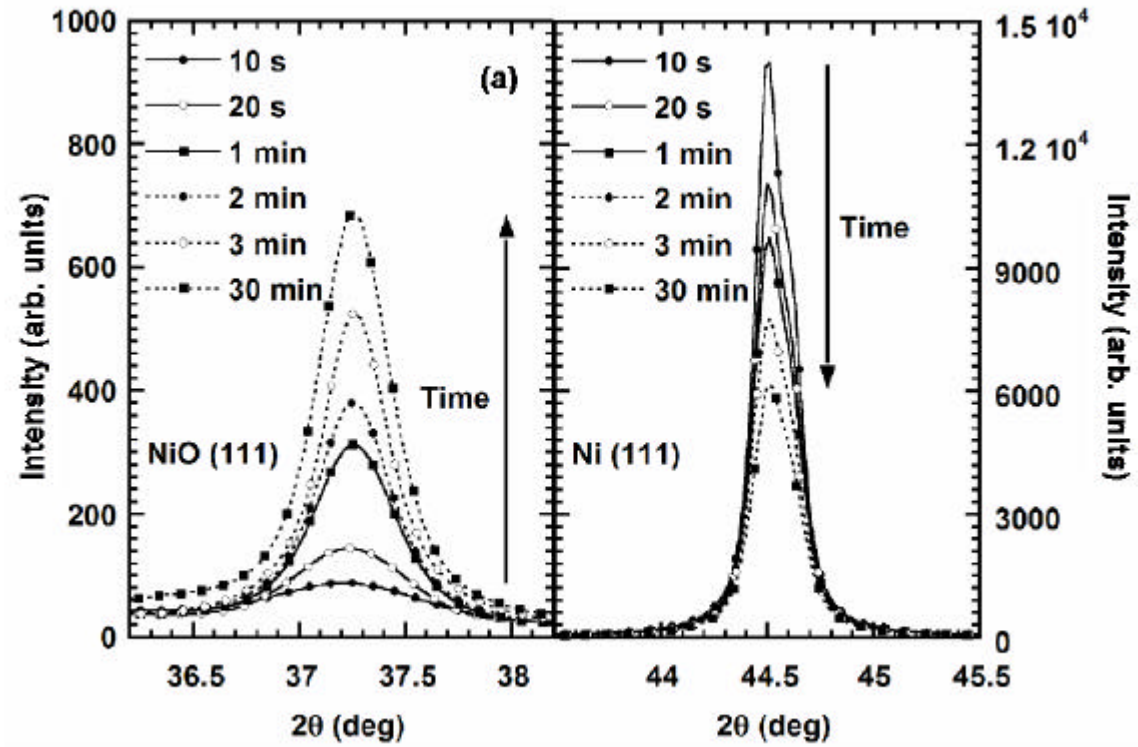
(a)
10 s
20 s
1 min
2 min
3 min
30 min
Time
NiO (111)
Ni (111)
Intensity (arb. units)
2θ (deg)
1000
800
600
400
200
0
36.5
37
37.5
38
44
44.5
45
45.5
1.5 10^4
1.2 10^4
9000
6000
3000

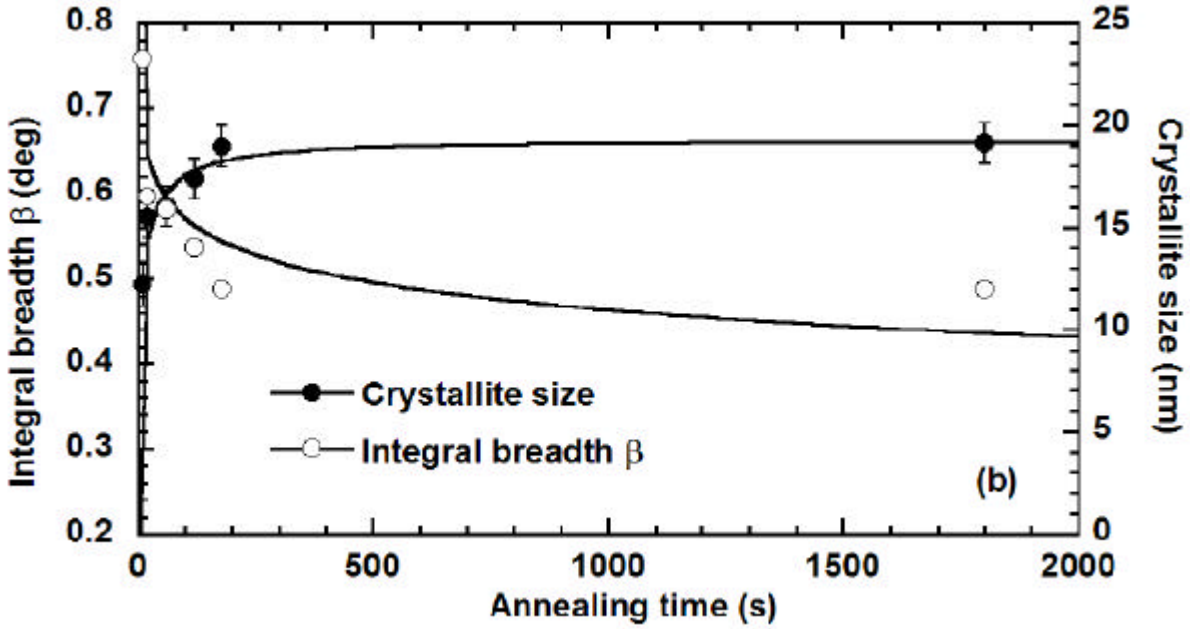
0.8
0.7
0.6
0.5
0.4
0.3
0.2
Integral breadth β (deg)
25
20
15
10
5
0
Crystallite size (nm)
0
500
1000
1500
2000
Annealing time (s)
Crystallite size
Integral breadth β
(b)

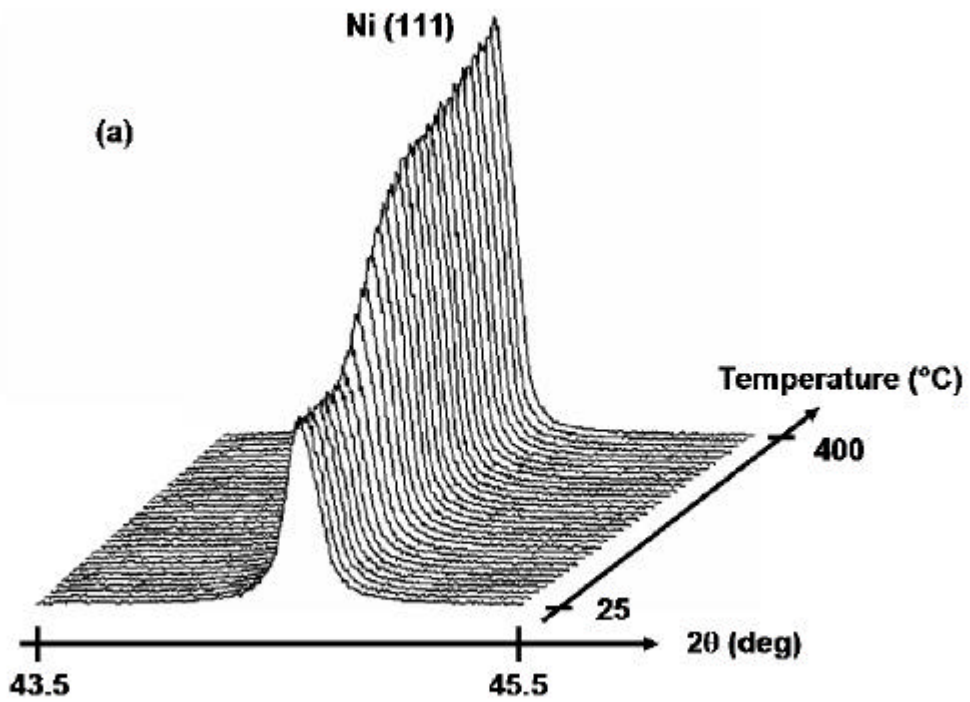
Ni (111)
(a)
Temperature (°C)
400
25
2θ (deg)
43.5
45.5

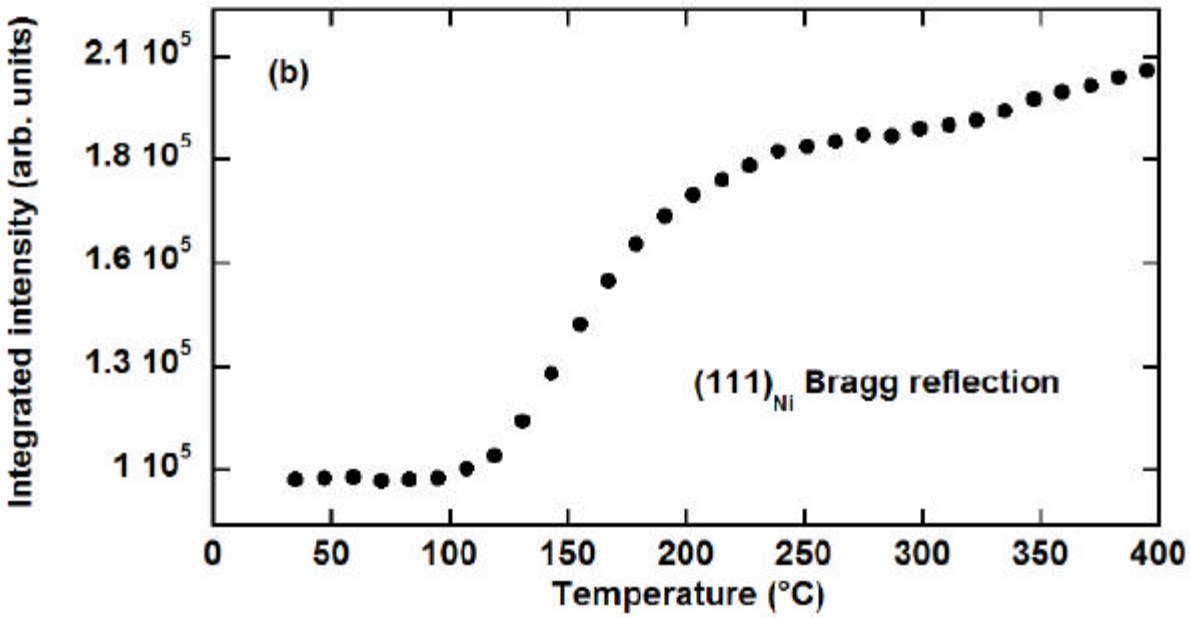
(b)
Integrated intensity (arb. units)
2.1 10^5
1.8 10^5
1.6 10^5
1.3 10^5
1 10^5
(111)Ni Bragg reflection
0
50
100
150
200
250
300
350
400
Temperature (°C)

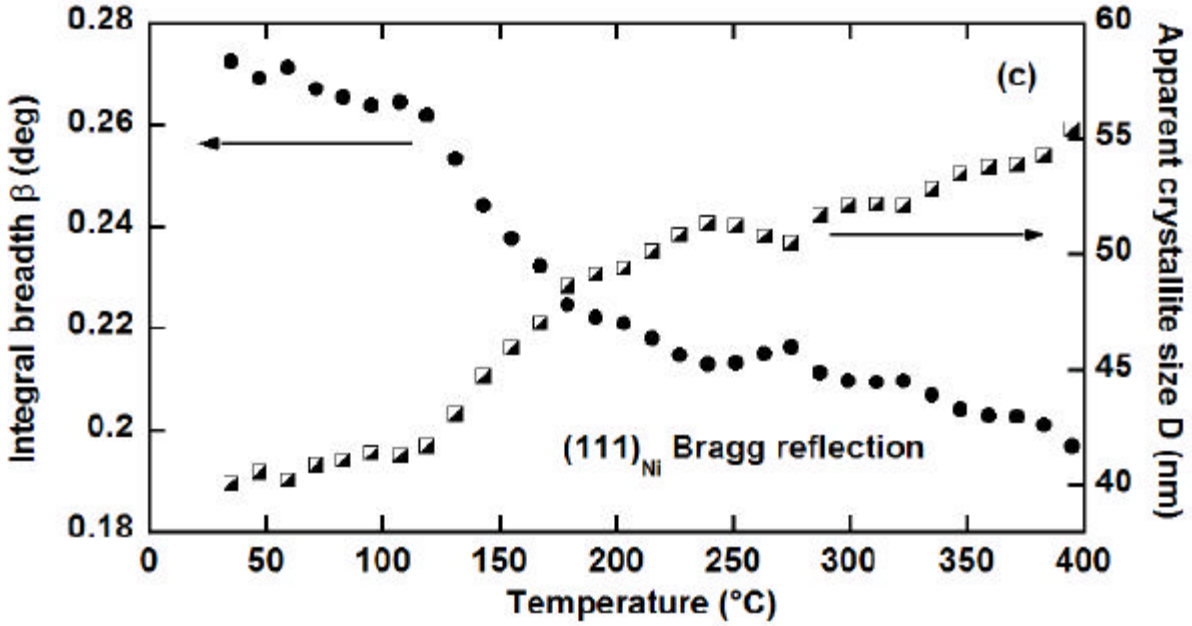
(c)
(111)Ni Bragg reflection
Integral breadth β (deg)
Apparent crystallite size D (nm)
Temperature (°C)
0.28
0.26
0.24
0.22
0.2
0.18
60
55
50
45
40
0
50
100
150
200
250
300
350
400

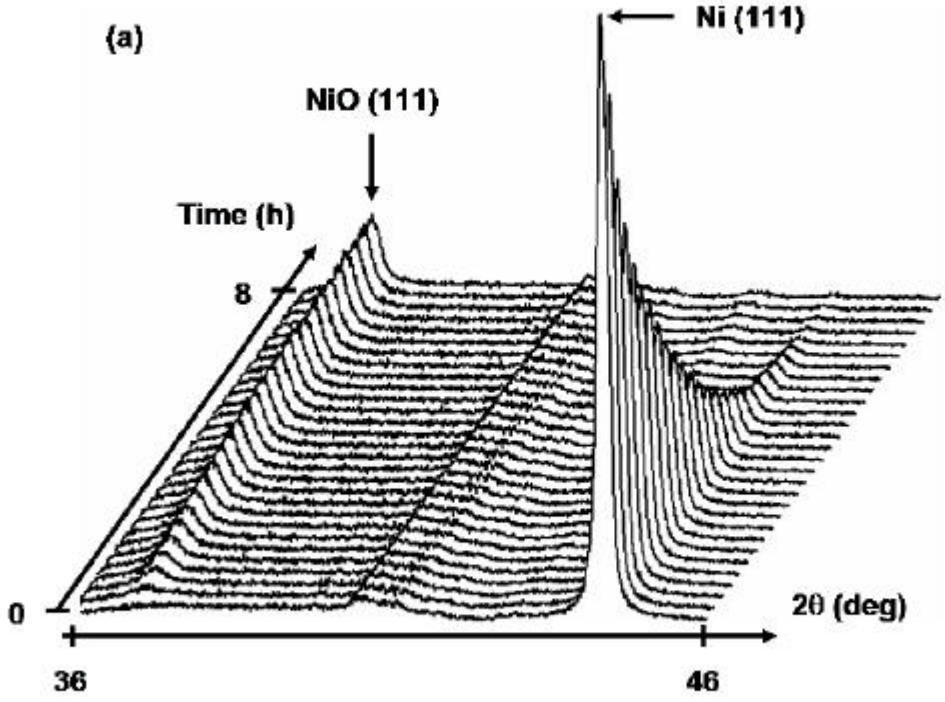
(a)
Ni (111)
NiO (111)
Time (h)
8
0
2θ (deg)
36
46

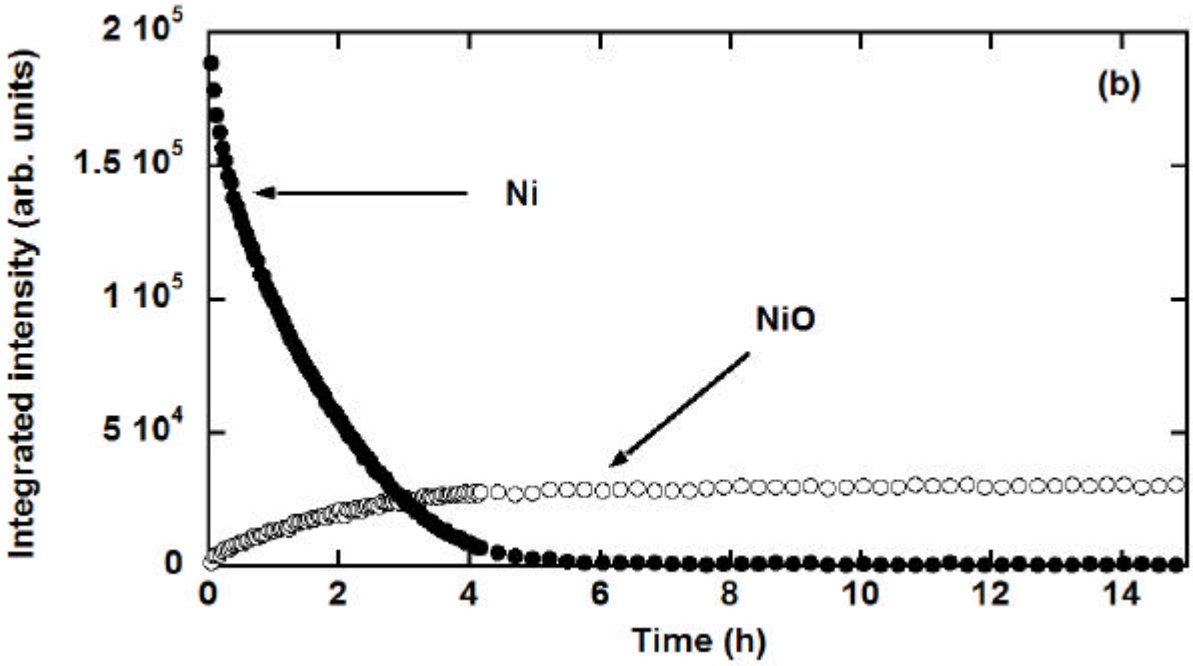
(b)
Ni
NiO
Integrated intensity (arb. units)
Time (h)
2 10^5
1.5 10^5
1 10^5
5 10^4
0
0
2
4
6
8
10
12
14

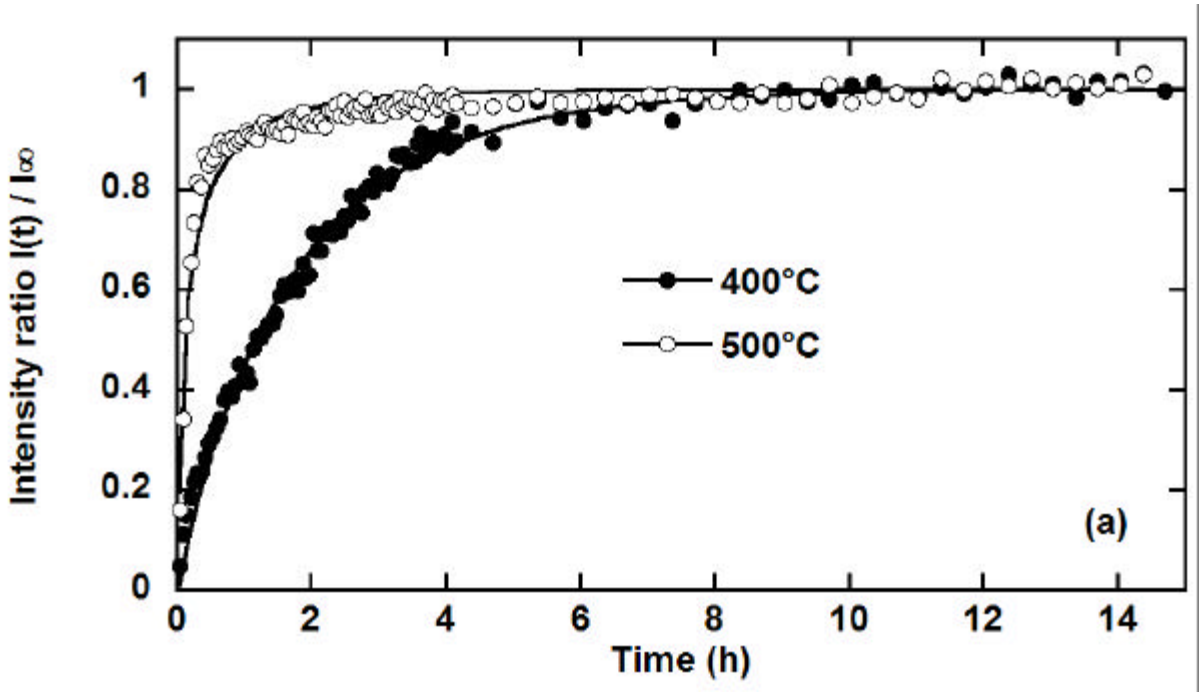
Intensity ratio I(t) / I∞
Time (h)
400°C
500°C
(a)
0
0.2
0.4
0.6
0.8
1
0
2
4
6
8
10
12
14

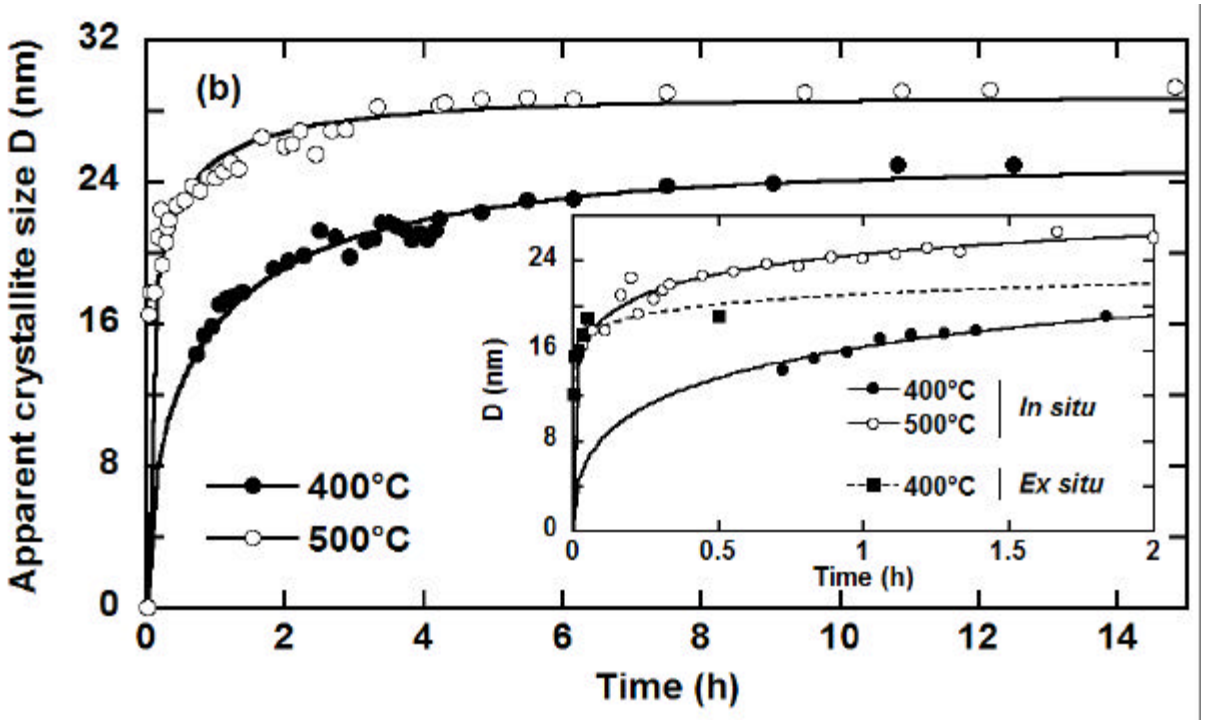
(b)
Apparent crystallite size D (nm)
Time (h)
400°C
500°C
D (nm)
Time (h)
400°C
500°C
In situ
400°C
Ex situ

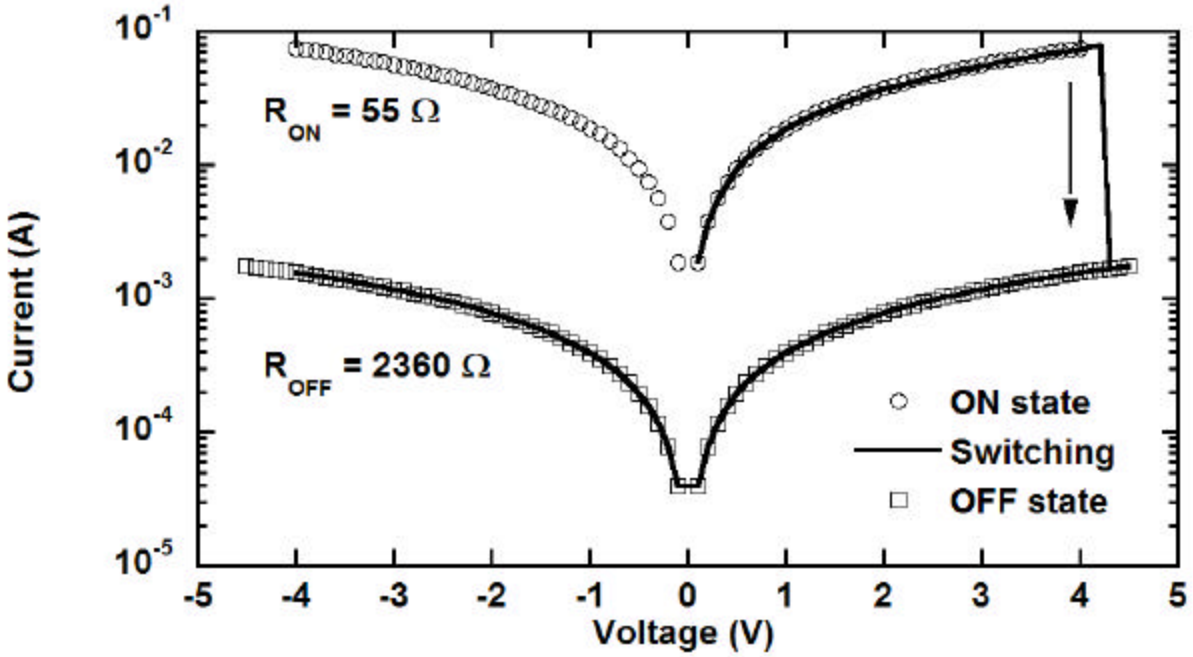
10^{-1}
10^{-2}
10^{-3}
10^{-4}
10^{-5}
Current (A)
R_{ON} = 55 Ω
R_{OFF} = 2360 Ω
ON state
Switching
OFF state
-5
-4
-3
-2
-1
0
1
2
3
4
5
Voltage (V)

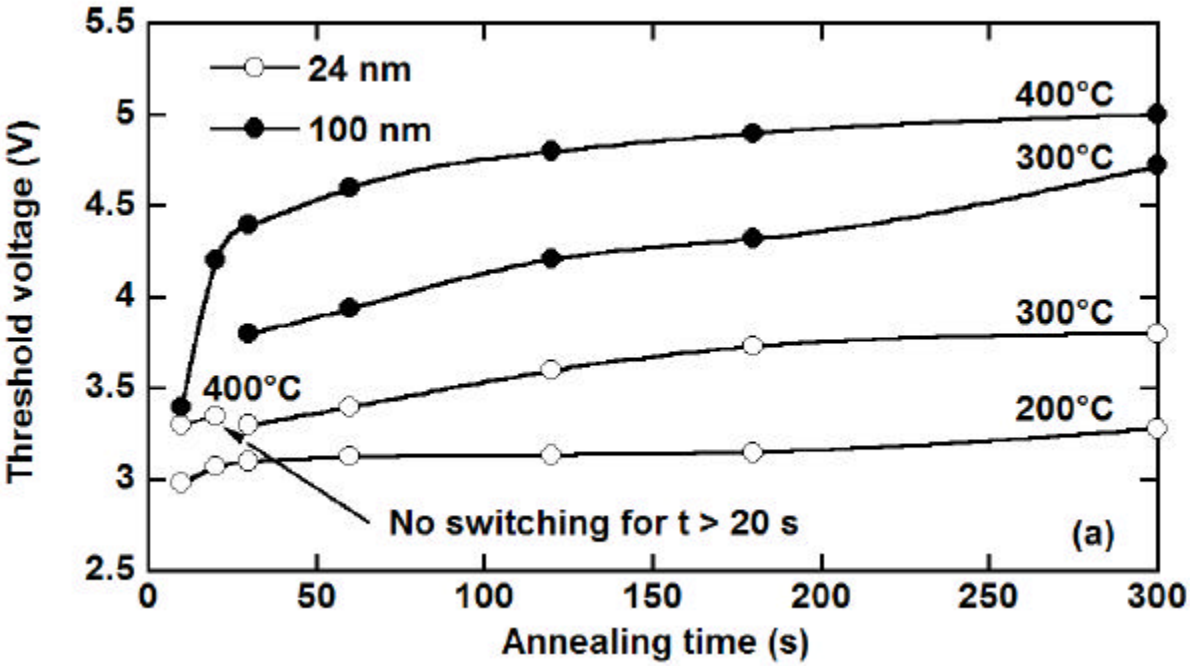
24 nm
100 nm
400°C
300°C
300°C
200°C
400°C
No switching for t > 20 s
(a)
Threshold voltage (V)
Annealing time (s)
5.5
5
4.5
4
3.5
3
2.5
0
50
100
150
200
250
300

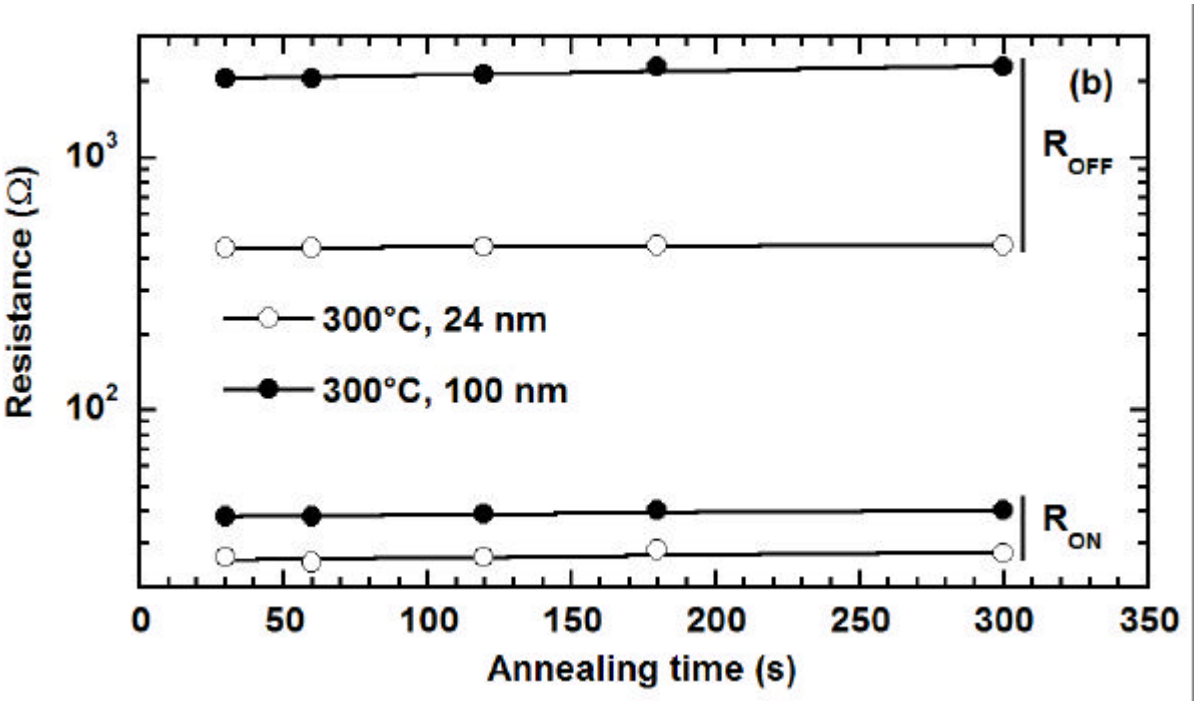
(b)
R_{OFF}
R_{ON}
300°C, 24 nm
300°C, 100 nm
Resistance (Ω)
10^3
10^2
0
50
100
150
200
250
300
350
Annealing time (s)

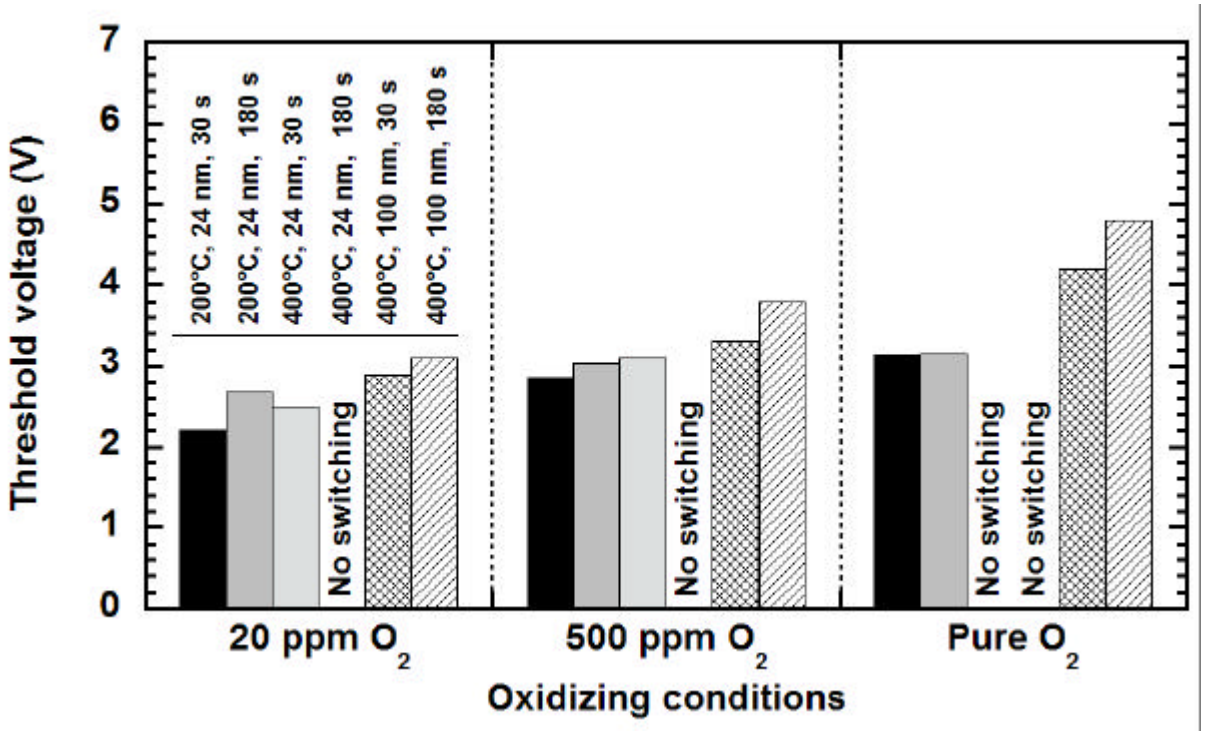
Threshold voltage (V)
0
1
2
3
4
5
6
7
200°C, 24 nm, 30 s
200°C, 24 nm, 180 s
400°C, 24 nm, 30 s
400°C, 24 nm, 180 s
400°C, 100 nm, 30 s
400°C, 100 nm, 180 s
No switching
No switching
No switching
No switching
20 ppm O2
500 ppm O2
Pure O2
Oxidizing conditions